Rare Met. (2022) 41(6):2055–2062
https://doi.org/10.1007/s12598-022-01974-7

RARE METALS

LETTER

Co single atoms and nanoparticles dispersed on N-doped carbon nanotube as high-performance catalysts for Zn-air batteries

Jing-Jing Chen, Shuai Gu, Rui Hao, Zhen-Yu Wang, Mu-Qing Li, Zhi-Qiang Li, Kun Liu, Ke-Meng Liao, Zhi-Qiang Wang, He Huang, Ying-Zhi Li, Kai-Li Zhang, Zhou-Guang Lu*

Received: 28 October 2021 / Revised: 22 November 2021 / Accepted: 1 December 2021 / Published online: 2 April 2022

Diminishing the size of active sites in catalysts is promising to improve the kinetics of oxygen reduction reaction (ORR) and reduce the cost of metal–air batteries. However, the facile preparation of high-performance catalysts with nanoscale active sites still suffers from great challenge. Herein, we report a facile template-free strategy to fabricate Co single atoms and nanoparticles dispersed on porous N-doped carbon nanotube (Co-NCNT) by the pyrolysis of the composites of metal–organic complexes and porous carbon nanotube. Different from the conventional strategy, the precursor metal–organic complexes in this work were prepared under mild conditions and used without complex purification procedures. Compared with the pristine carbon nanotube, N-doped carbon nanotube with abundant mesopores contribute to the formation of nanoscale Co sites. This resultant electrocatalyst Co-NCNT shows an impressive ORR half-wave potential of 0.87 V in alkaline solution, outperforming that of commercial Pt/C (20 wt%). The catalyst Co-NCNT displays high tolerance to strong alkali solution, endowing the aqueous Zn-air batteries with high discharge voltages and power density. In addition, the specific capacity achieves 803 mAh·g_{Zn}^{-1} under a current density of 10 mA·cm^{-1}. This research provides a new solution for the simple synthesis of carbon-based electrocatalysts for metal–air batteries.

Nowadays, in order to deal with the environmental issue caused by carbon pollution, metal–air batteries and fuel cells are considered as promising technologies to replace the fossil fuel economy [1–5]. High-performance electrocatalysts play an important role in improving the efficiency of cathodic oxygen reduction reaction (ORR) to convert chemical energy into electric energy for these batteries [6–14]. Although Pt-based catalysts exhibit excellent catalytic activity, their large-scale applications are limited by high cost, large overpotential loss, low stability, and low methanol tolerance [15–20]. Therefore, the development of new electrocatalysts is very important for the next generation energy conversion device.

Considering that reactions are dominated by the accessible surface atoms of the active sites in catalysts and the inaccessible inner atoms of the active sites contribute little to the reactions, diminishing the size of active sites in catalysts is very important to improve the reaction kinetics and reduce the cost of catalysts [21–24]. In recent years, nanoscale and single-atom metal sites in catalysts with high catalytic activity have been studied to replace the expensive Pt-based catalysts [25–31]. However, these nanoscale active sites are highly unstable and prone to aggregate influenced by their high surface free energy [32–34]. In the process of preparing carbon-loaded capsules, nanoscale active sites usually gather to form large particles at high temperature, and the catalyst must undergo chemical etch to remove large particles [35–37]. The supporting substrate can not only stabilize the energetic nanoscale active sites,

Supplementary Information The online version contains supplementary material available at https://doi.org/10.1007/s12598-022-01974-7.

J.-J. Chen, R. Hao, Z.-Y. Wang, M.-Q. Li, Z.-Q. Li, K. Liu, K.-M. Liao, Z.-Q. Wang, H. Huang, Y.-Z. Li, Z.-G. Lu*
Department of Materials Science and Engineering, Guangdong Provincial Key Laboratory of Energy Materials for Electric Power, Shenzhen Key Laboratory of Interfacial Science and Engineering of Materials, Southern University of Science and Technology, Shenzhen 518055, China
e-mail: luzg@sustech.edu.cn

S. Gu, K.-L. Zhang
Department of Mechanical Engineering, City University of Hong Kong, Hong Kong 999077, China

but can also involve the mass transfer in the electrocatalysis process, which is the pivotal component in the design of high-performance electrocatalyst. Thus, various porous and hollow carbon substrates have been prepared to anchor nanoscale metal sites [38–41]. However, it is still uneasy to obtain catalysts with nanoscale or single-atom metal sites. And the preparation of the precursors (such as MOFs [42] and biomass gel [43]) for the catalysts often requires tedious procedures, such as hydrothermal treatments, lyophilization, and template methods, which need high cost and take a lot of time. Therefore, designing electrocatalysts with nanoscale and single-atom metal sites that can be easily synthesized is very important for the next generation energy conversion device.

In this paper, we reported an effective strategy to synthesize nanoscale and atomic Co sites dispersed on N-doped carbon nanotube. Porous N-doped carbon nanotubes (NCNTs) were prepared from the commercial carbon nanotubes through a facile method and employed as supporting substrate to confine Co nanoparticles and Co-N_x active sites for the ORR. The chemical structure of the NCNTs was studied by Raman spectra, X-ray diffraction (XRD), X-ray photoelectron spectroscopy (XPS), and nitrogen adsorption/desorption experiments. Aberration-corrected high-angle annular dark-field scanning transmission electron microscopy (HAADF-STEM) and Co K-edge X-ray absorption fine structure (XAFS) spectra were used to confirm the Co nanoparticles and Co-N_x sites. Experimental results show that the catalyst Co-NCNT exhibits better electrocatalytic activity and stability than the commercial Pt/C in alkaline media for the ORR. The Zn-air batteries with the Co-NCNT catalyst exhibit high voltage, specific energy density and long-term stability.

The catalysts were synthesized via a facile two-step procedure (Fig. 1a) where the substrate porous NCNTs were synthesized by the KOH activation method according to literature methods [44, 45]. A composite catalyst involving Co complexes being encapsulated in NCNTs was synthesized through a facile, scalable route using cobalt acetate as Co precursors. The Co complex was formed by the coordination of $[Co(CH_3CO_2)_2]\cdot 4H_2O$ and o-phenylenediamine [46], which could disperse Co sites in advance. Through the dissolution and dispersion process of Co complex in solution, metal-containing precursor was trapped in the N-doped-carbon nanotubes substrates. In this process, the coordination could further disperse the metal atoms and make them separated uniformly to obtain the nanoparticles and single atoms in catalyst Co-NCNT. The sample Co-CNT were prepared by the pyrolysis of the mixture of Co complexes and pristine CNT. As shown in Fig. 1b, nitrogen adsorption/desorption curves at 77 K were collected to calculate the Brunauer–Emmett–Teller (BET) surface areas. The sample NCNT after the activation process displayed high BET surface area up to 386 $m^2\cdot g^{-1}$, higher than that of the pristine CNT (171 $m^2\cdot g^{-1}$). The sample Co-CNT exhibited lower BET surface area of 161 $m^2\cdot g^{-1}$ than the pristine CNT and the sample Co-NCNT (220 $m^2\cdot g^{-1}$). Compared with the sample Co-CNT, the increase in the specific surface area of Co-NCNT was attributed to the utilization of NCNT with high surface area, which contributed to expose more active sites and improve the catalytic performance. Pore size distribution curves (Fig. 1c) showed that Co-NCNT and NCNT had more mesopores (2–50 nm) than the pristine CNT and the sample Co-CNT, which may promote the mass transfer during the electrocatalytic process.

Powder X-ray diffraction (PXRD) demonstrates that the crystalline texture of NCNT is well maintained after the activation treatment and similar to that of the pristine CNT (Fig. 1d). XRD pattern of the sample Co-CNT displayed the characteristic peaks of metallic Co (JCPDS No. 15–0806) [47], implying the serious agglomeration of the Co species during the thermal treatment process. However, the crystalline characteristic peaks of Co species were not observed in the XRD pattern of the sample Co-NCNT, indicating that the Co species were well dispersed on the NCNT. As shown in Raman spectra (Fig. 1e), all the four samples had two broad peaks at around 1350 and 1580 cm^{-1}, which were attributed to typical G and D bands of graphitized and disordered carbons, respectively [48]. The intensity ratios (I_D/I_G) were 1.33, 2.00, 1.64 and 1.78 for CNT, NCNT, Co-CNT and Co-NCNT, respectively. The NCNT showed a larger I_D/I_G value than CNT, which indicated NCNT had more defects than CNT. Similarly, Co-NCNT had more defects than Co-CNT. Compared with the scanning electron microscope (SEM) pictures of the CNT (Fig. S1), the Co-NCNT (Fig. 1f) exhibited a shorter rod-like shape and a rougher surface. Circled areas in the high-resolution transmission electron microscope (HRTEM) pictures (Fig. 1g and Fig. S2) of Co-NCNT revealed that the ordered structures of the pristine CNT were partly damaged during the activation process, which was in good agreement with the results of Raman spectra. Inductively coupled plasma atomic emission spectrometry (ICP-AES) demonstrated the mass percent of cobalt element in Co-NCNT sample was 2.01 wt% ± 0.02 wt%.

XPS measurement was utilized to detect the chemical components of Co-NCNT (Fig. S3), confirmed the existence of C, N, O and Co elements. According to the XPS measurement, the N content in Co-NCNT was 4.68 wt%. The high-resolution N 1s spectra of Co-NCNT (Fig. S4) could be deconvoluted into four types of N species, pyridinic N (398.5 eV), graphitic N (401.1 eV), pyrrolic N (399.3 eV) and oxidized N (405.1 eV), respectively. In the Co 2p spectra (Fig. S5) of Co-NCNT, the peaks at 778.5 and 793.7 eV were assigned to Co metal, while peaks at

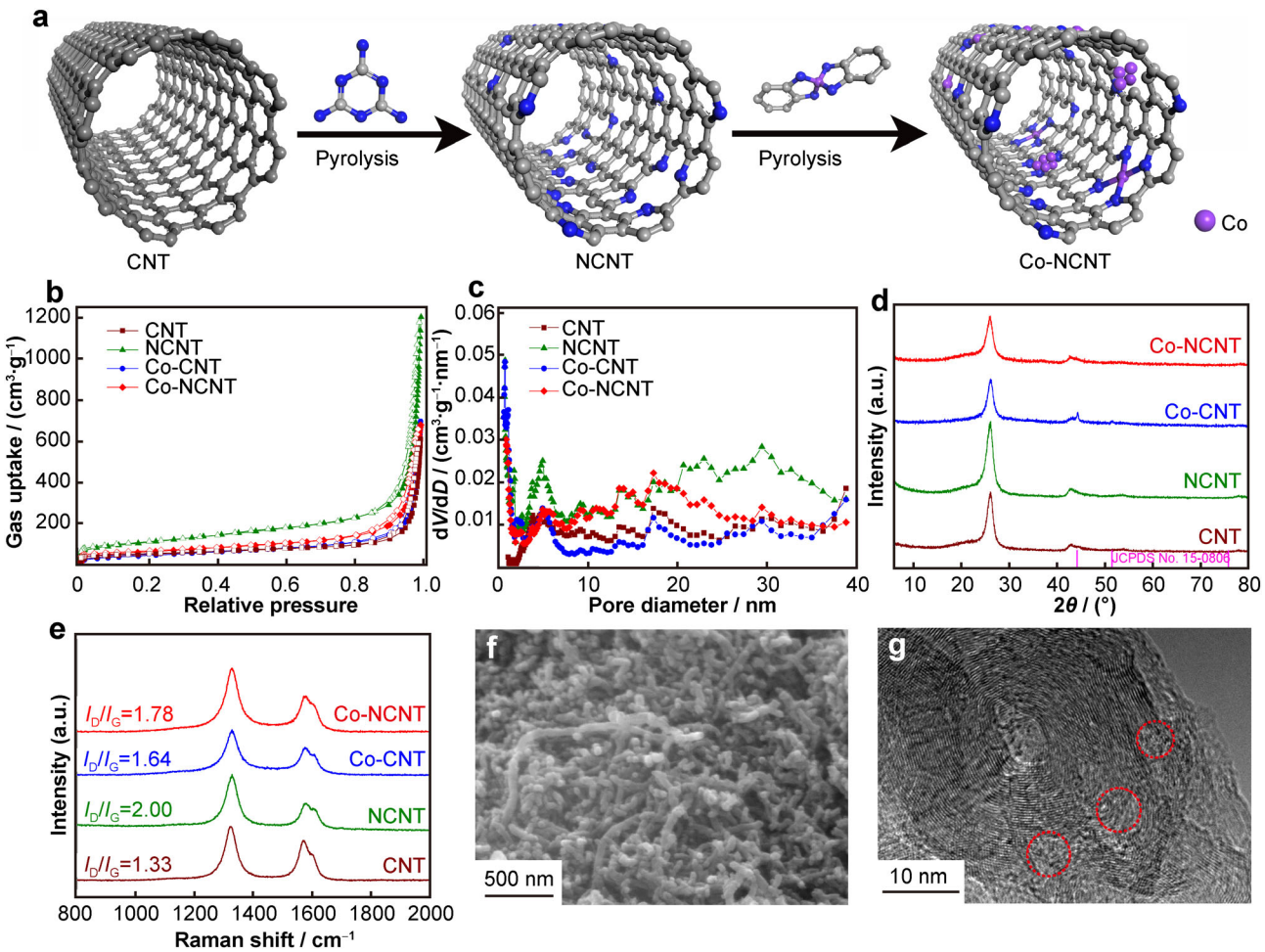

Fig. 1 **a** Schematic illustration of preparation, **b** nitrogen adsorption/desorption curves, **c** pore size distribution curves, **d** XRD patterns, **e** Raman spectra, **f** SEM image and **g** HRTEM image of Co-NCNT

780.1 and 795.7 eV were attributed to N-coordinated Co atoms (Co–N) [49]. High-resolution TEM images (Fig. 2a) of Co-NCNT showed the existence of nanoparticles with the major sizes less than 20 nm. Further analysis of the lattice fringes of the nanoparticles (Fig. 2b) demonstrated that the interspacing of 0.205 nm was assigned to the {111} lattice planes of Co metal. In contrast, the TEM images of the sample Co-CNT (Fig. S6) obtained from the pristine CNT directly displayed Co nanoparticles with the size larger than 20 nm, indicating that the porous NCNT with abundant N atoms contributed to effectively dispersing the Co sites. HAADF-STEM image of Co-NCNT showed that atomically isolated Co atoms (brighter dots) could be observed on the carbon matrix (Fig. 2c). As shown in Fig. 2d, elemental mapping images confirmed C, Co and N elements were homogeneously distributed in the Co-NCNT. X-ray absorption near-edge spectra (XANES) and the Fourier transform (FT) of XAFS spectra were collected to investigate the coordination structure and chemical state of Co atoms. As shown in Fig. 2e, the near-edge absorption position of Co K-edge of Co-NCNT was higher than that of Co foil, indicating that some Co atoms in the Co-NCNT possessed positive charge [50], which agrees with the XPS results. FT EXAFS spectrum of Co-NCNT at Co K-edge exhibited Co–N peaks at 0.146 nm and Co–Co peak at 0.125 nm (Fig. 2f), suggesting the existence of Co-N_x sites and Co nanoparticles [51], respectively, in accordance with the results of XPS and TEM. By comparing the samples Co-NCNT and Co-CNT, the results indicated that the doped N atoms in CNTs could disperse the Co active sites, facilitating the formation of Co single atoms and nanoparticles.

The ORR activity tests of Co-NCNT were evaluated by cyclic voltammetry (CV) and steady-state linear sweep voltammetry (LSV) in O_2-saturated 0.1 mol·L^{-1} KOH at room temperature. The CV curve (Fig. S7) in the Ar-saturated solution showed no obvious peaks for Co-NCNT sample. In contrast, in the O_2-saturated solution, Co-NCNT sample exhibited a distinct oxygen reduction peak, demonstrating good ORR catalytic activity. As shown in

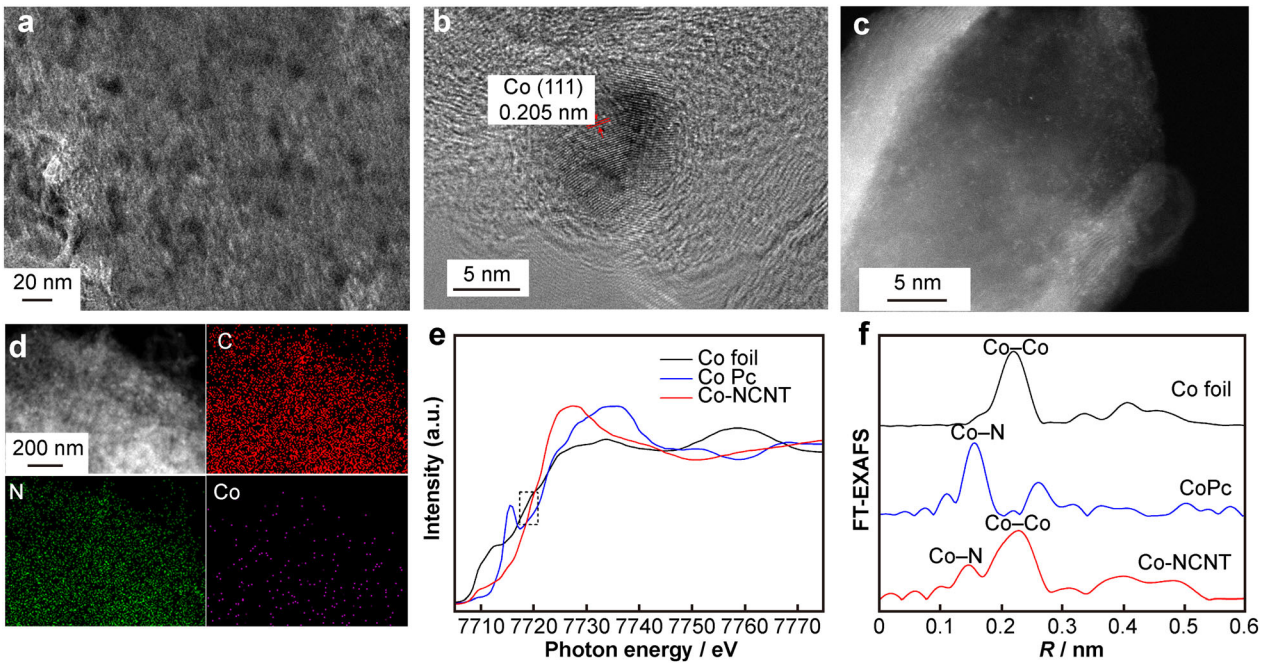

Fig. 2 **a** HRTEM image, **b** lattice fringes of Co nanoparticles, **c** HAADF-STEM image, **d** EDX elemental mappings of C (red), N (green), and Co (pink), **e** XANES spectra and **f** Fourier-transformed (FT) k^3-weighted spectra of Co-NCNT

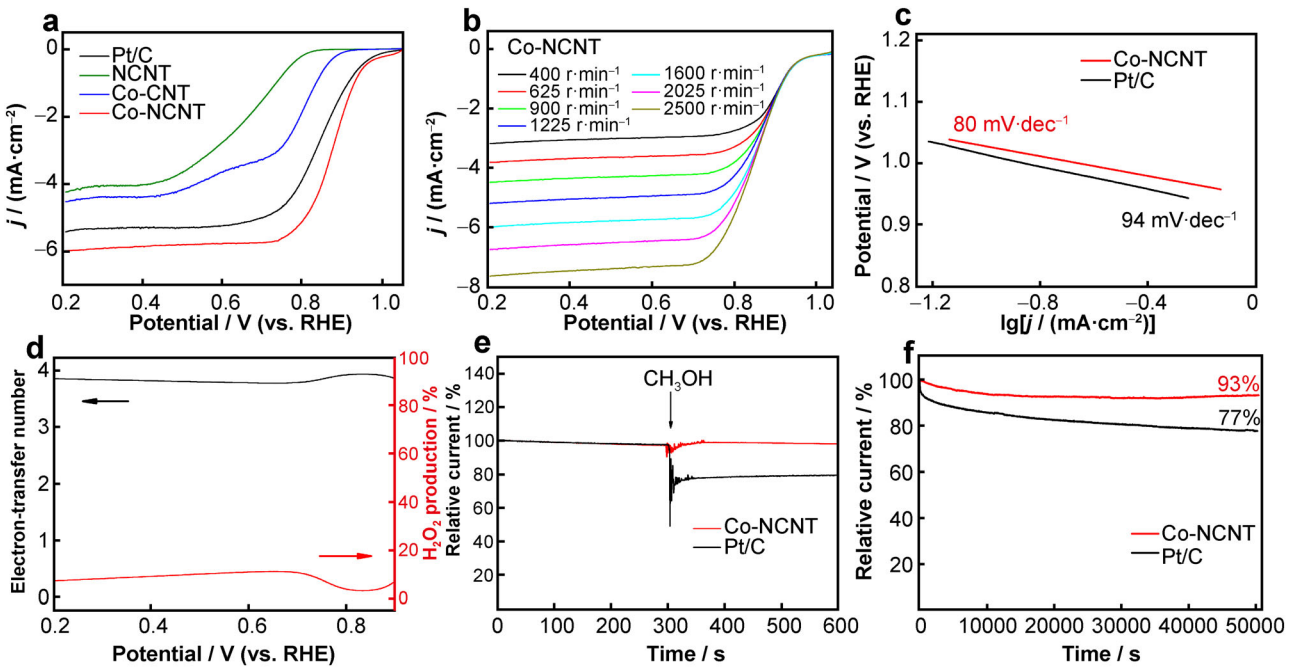

Fig. 3 **a** ORR polarization plots of NCNT, Co-CNT, Co-NCNT and Pt/C; **b** ORR polarization curves for Co-NCNT at various rotation speeds with 10 mV·s^{-1}; **c** Tafel slopes at 1600 r·min^{-1} of Co-NCNT and Pt/C; **d** electron transfer numbers (left) and H_2O_2 yield (right) of Co-NCNT at various potentials; **e** tolerance to methanol of Co-NCNT compared with 20 wt% Pt/C at 0.60 V; **f** stability test for Co-NCNT and Pt/C at 0.6 V (vs. RHE)

Fig. 3a, without Co doping, the NCNT catalyst displayed a poor ORR activity with half-wave potential ($E_{1/2}$) of 0.63 V (vs. RHE). And Co-CNT with Co doping but no nitrogen atoms displayed significantly better ORR activity ($E_{1/2}$ = 0.76 V) than NCNT. This result illustrated that the metal species as the active sites in Co-CNT possessed obvious advantages for electrocatalytic ORR compared with the non-metal sites in NCNT. By contrast, Co-NCNT

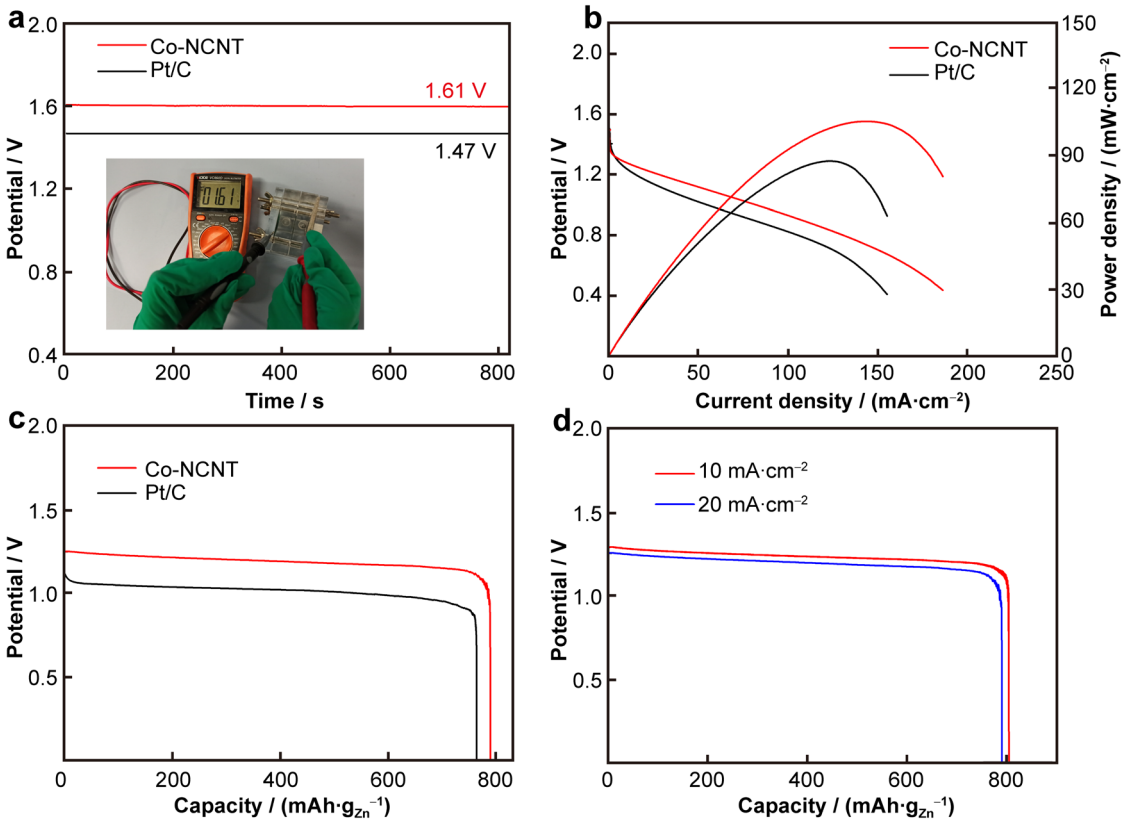

Fig. 4 **a** Voltage–time curves of Co-NCNT and Pt/C; **b** discharge polarization plots and power density of Zn-air batteries using Co-NCNT and Pt/C as ORR catalysts in 6 mol·L^{-1} KOH electrolyte; **c** voltage-capacity curves of Zn-air batteries with Co-NCNT and Pt/C catalysts at 20 mA·cm^{-2}; **d** voltage-capacity curves of Zn-air batteries with Co-NCNT catalyst at 10 and 20 mA·cm^{-2}

(with Co and N doping) displayed the highest ORR activity ($E_{1/2}$ = 0.87 V), better than commercial Pt/C (0.84 V). This could be attributed to that the porous N-doping NCNT substrate could effectively disperse the Co species, which has been demonstrated by TEM and HAADF-STEM images. After etching the catalyst Co-NCNT by acid solution, the obtained catalyst Co-NCNT-a exhibited a relative low content of Co nanoparticles compared with Co-NCNT, which was demonstrated by the XPS spectra (Figures S5, S8). The catalyst Co-NCNT-a showed a half-wave potential of 0.83 V (Figure S9), lower than that of the pristine catalyst Co-NCNT (0.87 V) without acid treatment but close to that of the commercial catalyst Pt/C (0.84 V). This indicated that the synergistic effect of Co single atoms and nanoparticles contributed to improving the electrocatalytic performance.

The rotating disk electrode (RDE) tests with various rotation rates from 400 to 2500 r·min^{-1} (Fig. 3b) can confirm that the ORR on the novel Co-NCNT catalyst was the four-electron process. And the electron transfer number (n) based on the linear Koutecky–Levich (K-L) equation was calculated to be 3.85 at 0.35 V (vs. RHE) (Fig. S10). The outstanding ORR catalytic activity can also be proofed by Tafel plots, exhibiting a smaller slope than Pt/C, indicating its fast kinetics in the oxygen reduction process (Fig. 3c). The H_2O_2 yield and the electron transfer number (n) of Co-NCNT catalyst were determined by the rotating ring-disk electrodes (RRDE) tests, and the values were about 8% and 3.86, respectively (Fig. 3d). This result indicates the ORR process on the Co-NCNT catalyst was dominated by the four-electron ($4e^-$) ORR pathway, in accordance with the results of the K-L plots. The Co-NCNT also exhibited a strong tolerance for methanol and outstanding stability measured by chronoamperometric (CA) tests. The current–time (i-t) chronoamperometric responses further confirmed the excellent stability of the Co-NCNT. As shown in Fig. 3e, after the methanol was added, the Co-NCNT could maintain a quite stable current density, while the commercial Pt/C appeared a sharp jump. At 0.60 V (vs. RHE), the current density of the ORR on the Co-NCNT catalyst displayed a 93% retention over 50,000 s, while the commercial catalyst 20 wt% Pt/C showed a 77% retention in current density (Fig. 3f). All these results demonstrated the high stability and outstanding electrocatalytic activity of the designed Co-NCNT material.

The catalyst Co-NCNT was further applied in Zn-air cell as air cathodes to evaluate the practical application. In the

assembled battery device (Fig. S11), a zinc plate was utilized as the anodes and 6 mol·L^{-1} KOH was utilized as the electrolyte. The open circuit voltage of the Zn-air battery with the Co-NCNT catalyst was 1.61 V (Fig. 4a), higher than that of the commercial 20 wt% Pt/C catalyst (1.47 V). The voltage-current polarization curves (Fig. 4b) demonstrated the excellent performance of the catalyst Co-NCNT for Zn-air batteries, which exhibited a maximum power density of 105.5 mW·cm^{-2} at 145.2 mA·cm^{-2}, surpassing that of the Pt/C-based device (87.6 mW·cm^{-2} at 122.6 mA·cm^{-2}). The specific capacity of Co-NCNT-based battery was 789 mAh·g_{Zn}^{-1} at 20 mA·cm^{-1} (Fig. 4c), while that of the Pt/C-based device was 762 mAh·g_{Zn}^{-1}. At 10 mA·cm^{-1}, the battery could display a capacity of 803 mAh·g_{Zn}^{-1} (Fig. 4d). These results indicated that Co-NCNT with high activity and stability was a promising competitor to replace the commercial Pt/C catalyst for the ORR in Zn-air batteries.

In summary, porous N-doped carbon nanotube has been reported to disperse the Co nanoparticles and single atoms by an effective strategy. The dispersed Co nanoparticles and single atoms sites of the Co-NCNT catalyst were verified by TEM, XPS, aberration-corrected HAADF-STEM and XAFS measurements. The Co-NCNT catalyst displayed better activity and stability than the commercial Pt/C catalyst for ORR. Moreover, the primary Zn-air batteries with Co-NCNT catalyst displayed high power density and stability, which demonstrated its practical application. This work provides an important reference for the design and preparation of highly dispersed metal sites in catalysts for high-performance energy storage and conversion devices.

Acknowledgements This work was financially supported by the National Natural Science Foundation of China (No. 21875097), the Basic Research Project of the Science and Technology Innovation Commission of Shenzhen (Nos. JCYJ20200109141640095 and No. JCYJ20190809115413414), Shenzhen Key Laboratory of Interfacial Science and Engineering of Materials (No. ZDSYS20200421111401738), the Leading Talents of Guangdong Province Program (No. 2016LJ06C536) and Guangdong-Hong Kong-Macao Joint Laboratory (No. 2019B121205001). This work was also partially supported by Hong Kong Research Grants Council (No. CityU 11218420). TEM and HAADF-STEM images were collected on the instruments from the Southern University of Science and Technology Core Research Facilities.

Declarations

Conflict of interests The authors declare that they have no conflict of interest.

References

[1] Zhao Y, Zhang L, Liu J, Adair K, Zhao F, Sun Y, Wu T, Bi X, Amine K, Lu J, Sun X. Atomic/molecular layer deposition for energy storage and conversion. Chem Soc Rev. 2021;50(6):3889.
[2] Zhao Q, Yan Z, Chen C, Chen J. Spinels: controlled preparation, oxygen reduction/evolution reaction application, and beyond. Chem Rev. 2017;117(15):10121.
[3] Wang LP, Shen QX, Tian L, Yang N, Xie G, Li B. Preparation of PtCo composite nanowires and characterization of electrocatalytic performance for oxygen reduction reaction. Chin J Rare Met. 2019;43(4):367.
[4] Huang X, Shen T, Sun S, Hou Y. Synergistic modulation of carbon-based, precious-metal-free electrocatalysts for oxygen reduction reaction. ACS Appl Mater Interf. 2021;13(6):6989.
[5] Du C, Liu X, Ye G, Gao X, Zhuang Z, Li P, Xiang D, Li X, Clayborne AZ, Zhou X, Chen W. Balancing the micro-meso-porosity for activity maximization of N-doped carbonaceous electrocatalysts for the oxygen reduction reaction. Chemsuschem. 2019;12(5):1017.
[6] Li H, Shu X, Tong P, Zhang J, An P, Lv Z, Tian H, Zhang J, Xia H. Fe–Ni alloy nanoclusters anchored on carbon aerogels as high-efficiency oxygen electrocatalysts in rechargeable Zn–air batteries. Small. 2021;17(36):2102002.
[7] Hu L, Gu S, Yu W, Zhang W, Xie Q, Pan C, Tang J, Yu G. Facile preparation of CoO nanoparticles embedded N-doped porouscarbon from conjugated microporous polymer for oxygen reduction reaction. J Colloid Interface Sci. 2020;562:550.
[8] Shi J, Shu X, Xiang C, Li H, Li Y, Du W, An P, Tian H, Zhang J, Xia H. Fe ultra-small particles anchored on carbon aerogels to enhance the oxygen reduction reaction in Zn-air batteries. J Mater Chem A. 2021;9(11):6861.
[9] Hao R, Chen J, Wang Z, Zhang J, Gan Q, Wang Y, Li Y, Luo W, Wang Z, Yuan H, Yan C, Zheng W, Huang Y, Liu P, Yan J, Liu K, Liu C, Lu Z. Iron polyphthalocyanine-derived ternary-balanced Fe_3O_4/Fe_3N/Fe-N-C@PC as a high-performance electrocatalyst for the oxygen reduction reaction. Sci China Mater. 2021;64:2987.
[10] Huang X, Shen T, Zhang T, Qiu H, Gu X, Ali Z, Hou Y. Efficient oxygen reduction catalysts of porous carbon nanostructures decorated with transition metal species. Adv Energy Mater. 2020;10(11):1900375.
[11] Shang C, Yang M, Wang Z, Li M, Liu M, Zhu J, Zhu Y, Zhou L, Cheng H, Gu Y, Tang Y, Zhao X, Lu Z. Encapsulated MnO in N-doping carbon nanofibers as efficient ORR electrocatalysts. Sci China Mater. 2017;60(10):937.
[12] Hao R, Gu S, Chen J, Wang Z, Gan Q, Wang Z, Huang Y, Liu P, Zhang K, Liu K, Liu C, Lu Z. Microporous Fe-N_4 catayst derived from biomass aerogel for a high-performance Zn-air battery. Mater Today Energy. 2021;21:100826.
[13] Cao L, Yang M, Lu Z, Pan H. Exploring an effective oxygen reduction reaction catalyst via $4e^-$ process based on waved--graphene. Sci China Mater. 2017;60(8):739.
[14] Huang X, Zhang Y, Shen H, Li W, Shen T, Ali Z, Tang T, Guo S, Sun Q, Hou Y. N-doped carbon nanosheet networks with favorable active sites triggered by metal nanoparticles as bifunctional oxygen electrocatalysts. ACS Energy Lett. 2018;3(12):2914.

[15] Hao R, Chen J, Wang Z, Huang Y, Liu P, Yan J, Liu K, Liu C, Lu Z. Trimetallic zeolitic imidazolite framework-derived Co nanoparticles@CoFe-nitrogen-doped porous carbon as bifunctional electrocatalysts for Zn-air battery. J Colloid Interface Sci. 2021;586:621.
[16] Wu S, Zhu Y, Huo Y, Luo Y, Zhang L, Wan Y, Nan B, Cao L, Wang Z, Li M, Yang M, Cheng H, Lu Z. Bimetallic organic frameworks derived CuNi/carbon nanocomposites as efficient electrocatalysts for oxygen reduction reaction. Sci China Mater. 2017;60(7):654.
[17] Qiao MF, Wang Y, Li L, Hu GZ, Zou GA, Mamat X, Dong YM, Hu X. Self-templated nitrogen-doped mesoporous carbon decorated with double transition-metal active sites for enhanced oxygen electrode catalysis. Rare Met. 2020;39(7):824.
[18] Huang K, Zhang W, Li J, Fan Y, Yang B, Rong C, Qi J, Chen W, Yang J. In situ anchoring of zeolite imidazole framework-derived Co, N-doped porous carbon on multiwalled carbon nanotubes toward efficient electrocatalytic oxygen reduction. ACS Sustain Chem Eng. 2020;8(1):478.
[19] Xiang D, Bo X, Gao X, Du C, Li P, Zhu L, Chen W. Bimetal- and nitrogen-codoped spherical porous carbon with efficient catalytic performance towards oxygen reduction reaction in alkaline media. J Colloid Interf Sci. 2019;534:655.
[20] Zhang R, He S, Lu Y, Chen W. Fe Co, N-functionalized carbon nanotubes in situ grown on 3D porous N-doped carbon foams as a noble metal-free catalyst for oxygen reduction. J Mater Chem A. 2015;3(7):3559.
[21] Peng Y, Lu B, Chen S. Carbon-supported single atom catalysts for electrochemical energy conversion and storage. Adv Mater. 2018;30(48):1801995.
[22] Chen Z, Wu R, Liu Y, Ha Y, Guo Y, Sun D, Liu M, Fang F. Ultrafine Co nanoparticles encapsulated in carbon-nanotubes-grafted graphene sheets as advanced electrocatalysts for the hydrogen evolution reaction. Adv Mater. 2018;30(30):1802011.
[23] Du C, Gao Y, Chen H, Li P, Zhu S, Wang J, He Q, Chen W. A Cu and Fe dual-atom nanozyme mimicking cytochrome c oxidase to boost the oxygen reduction reaction. J Mater Chem A. 2020;8(33):16994.
[24] Du C, Gao Y, Wang J, Chen W. A new strategy for engineering a hierarchical porous carbon-anchored Fe single-atom electrocatalyst and the insights into its bifunctional catalysis for flexible rechargeable Zn–air batteries. J Mater Chem A. 2020;8(19):9981.
[25] Zhang M, Qiu JJ, Yin T, Tan CL. Research progress and application prospect of silver nanoparticles and nanoporous silver materials. Chin J Rare Met. 2020;44(1):79.
[26] Chen Y, Gao R, Ji S, Li H, Tang K, Jiang P, Hu H, Zhang Z, Hao H, Qu Q, Liang X, Chen W, Dong J, Wang D, Li Y. Atomic-level modulation of electronic density at cobalt single-atom sites derived from metal-organic frameworks: enhanced oxygen reduction performance. Angew Chem Int Ed. 2021;60(6):3212.
[27] Xia H, Qu G, Yin H, Zhang J. Atomically dispersed metal active centers as a chemically tunable platform for energy storage devices. J Mater Chem A. 2020;8(31):15358.
[28] Shang H, Jiang Z, Zhou D, Pei J, Wang Y, Dong J, Zheng X, Zhang J, Chen W. Engineering a metal-organic framework derived Mn-N_4-C_xS_y atomic interface for highly efficient oxygen reduction reaction. Chem Sci. 2020;11(23):5994.
[29] Zhao X, Li YG. Two-electron oxygen reduction reaction by high-loading molybdenum single-atom catalysts. Rare Met. 2020;39(5):455.
[30] Peng L, Shang L, Zhang T, Waterhouse G. Recent advances in the development of single-atom catalysts for oxygen electrocatalysis and zinc-air batteries. Adv Energy Mater. 2020;10(48):2003018.
[31] Hou CC, Zou L, Sun L, Zhang K, Liu Z, Li Y, Li C, Zou R, Yu J, Xu Q. Single-atom iron catalysts on overhang-eave carbon cages for high-performance oxygen reduction reaction. Angew Chem Int Ed. 2020;59(19):7384.
[32] Wei X, Zheng D, Zhao M, Chen H, Fan X, Gao B, Gu L, Guo Y, Qin J, Wei J, Zhao Y, Zhang G. Cross-linked polyphosphazene hollow nanosphere-derived N/P-doped porous carbon with single nonprecious metal atoms for the oxygen reduction reaction. Angew Chem Int Ed. 2020;59(34):14639.
[33] Zhang H, Liu G, Shi L, Ye J. Single-atom catalysts: emerging multifunctional materials in heterogeneous catalysis. Adv Energy Mater. 2018;8(1):1701343.
[34] Lang R, Xi W, Liu JC, Cui YT, Li T, Lee AF, Chen F, Chen Y, Li L, Li L, Lin J, Miao S, Liu X, Wang AQ, Wang X, Luo J, Qiao B, Li J, Zhang T. Non defect-stabilized thermally stable single-atom catalyst. Nat Commun. 2019;10:234.
[35] Liu JC, Tang Y, Wang YG, Zhang T, Li J. Theoretical understanding of the stability of single-atom catalysts. Nat Sci Rev. 2018;5(5):638.
[36] Yang HB, Hung S-F, Liu S, Yuan K, Miao S, Zhang L, Huang X, Wang HY, Cai W, Chen R, Gao J, Yang X, Chen W, Huang Y, Chen HM, Li CM, Zhang T, Liu B. Atomically dispersed Ni(I) as the active site for electrochemical CO_2 reduction. Nat Energy. 2018;3:140.
[37] Tian H, Cui X, Dong H, Meng G, Kong F, Chen Y, Peng L, Chen C, Chang Z, Shi J. Enginering single MnN_4 atomic active sites on polydopamine-modified helical carbon tubes towards efficient oxygen reduction. Energy Storage Mater. 2021;37:274.
[38] Zhang S, Yang W, Liang Y, Yang X, Cao M, Cao R. Template-free synthesis of non-noble metal single-atom electrocatalyst with N-doped holey carbon matrix for highly efficient oxygen reduction reaction in zinc-air batteries. Appl Catal B Environ. 2021;285:119780.
[39] Han J, Bao H, Wang JQ, Zheng L, Sun S, Wang ZL, Sun C. 3D N-doped ordered mesoporous carbon supported single-atom Fe-N-C catalysts with superior performance for oxygen reduction reaction and zinc-air battery. Appl Catal B Environ. 2021;280:119411.
[40] Li H, Du K, Xiang C, An P, Shu X, Dang Y, Wu C, Wang J, Du W, Zhang J, Li S, Tian H, Wang S, Xia H. Controlled chelation between tannic acid and Fe precursors to obtain N, S co-doped carbon with high density Fe-single atom-nanoclusters for highly efficient oxygen reduction reaction in Zn–air batteries. J Mater Chem A. 2020;8(33):17136.
[41] Chen F, Wu XL, Shi C, Lin H, Chen J, Shi Y, Wang S, Duan X. Molecular engineering toward pyrrolic N-rich M-N_4 (M = Cr, Mn, Fe Co, Cu) single-atom sites for enhanced heterogeneous fenton-like reaction. Adv Funct Mater. 2021;31(13):2007877.
[42] Li Y, Zhou W, Zheng L, Liu J, Tang R, Shi K, Zhang Y. Hollow porous nitrogen-doped carbon formed by Fe-modified bimetallic organic framework for rechargeable liquid/solid Zn-air batteries. J Alloys Compd. 2021;886:161227.
[43] Wang L, Liang K, Deng L, Liu YN. Protein hydrogel networks: a unique approach to heteroatom self-doped hierarchically porous carbon structures as an efficient ORR electrocatalyst inboth basic and acidic conditions. Appl Catal B: Environ. 2019;246:89.
[44] Gu S, He J, Zhu Y, Wang Z, Chen D, Yu G, Pan C, Guan J, Tao K. Facile carbonization of microporous organic polymers into hierarchically porous carbons targeted for effective CO_2 uptake at low pressures. ACS Appl Mater Interf. 2016;8(28):18383.
[45] Zhu Y, Murali S, Stoller MD, Ganesh KJ, Cai W, Ferreira PJ, Pirkle A, Wallace RM, Cychosz KA, Thommes M, Su D, Stach EA, Ruoff RS. Carbon-based supercapacitors produced by activation of graphen. Science. 2011;332(6037):1537.

[46] Bill E, Bothe E, Chaudhuri P, Chlopek K, Herebian D, Kokatam S, Ray K, Weyhermüller T, Neese F, Wieghardt K. Molecular and electronic structure of four- and five-coordinate cobalt complexes containing two o-phenylenediamine- or two o--aminophenol-type ligands at various oxidation levels: an experimental, density functional, and correlated ab initio study. Chem Eur J. 2005;11(1):204.
[47] Leng D, Tang H, Yang M, Zhang J, Zhang Y, Qin J, Liu Q, Lu H, Yin F. Co/N-doped carbon nanotubes-grafted porous carbon sheets architecture as efficient electrocatalyst for oxygen reduction reaction. J Alloys Compd. 2021;871:159566.
[48] Wang ZY, Jiang SD, Duan CQ, Wang D, Luo SH, Liu YG. In situ synthesis of Co_3O_4 nanoparticles confined in 3D nitrogen doped porous carbon as an efficient bifunctional oxygen electrocatalyst. Rare Met. 2020;39(12):1383.
[49] Wang Z, Shen J, Ji S, Xu X, Zuo S, Liu Z, Zhang D, Hu R, Ouyang L, Liu J, Zhu M. B, N codoped graphitic nanotubes loaded with Co nanoparticles as superior sulfur host for advanced Li-S batteries. Small. 2020;16(7):1906634.
[50] Pan Y, Lin R, Chen Y, Liu S, Zhu W, Cao X, Chen W, Wu K, Cheong WC, Wang Y, Zheng L, Luo J, Lin Y, Liu Y, Liu C, Li J, Lu Q, Chen X, Wang D, Peng Q, Chen C, Li Y. Design of single-atom $Co-N_5$ catalytic site: a robust electrocatalyst for CO_2 reduction with nearly 100% CO selectivity and remarkable stability. J Am Chem Soc. 2018;140(12):4218.
[51] Xie X, He C, Li B, He Y, Cullen DA, Wegener EC, Kropf AJ, Martinez U, Cheng Y, Engelhard MH, Bowden ME, Song M, Lemmon T, Li XS, Nie Z, Liu J, Myers DJ, Zelenay P, Wang G, Wu G, Ramani V, Shao Y. Performance enhancement and degradation mechanism identification of a single-atom Co-N-C catalyst for proton exchange membrane fuel cells. Nat Catal. 2020;3:1044.